

Geometrically-Shaped Constellation for Visible Light Communications at Short Blocklength

Jia-Ning Guo, Ru-Han Chen*, Jian Zhang, Longguang Li, Xu Yang, and Jing Zhou

Abstract—In this paper, we present a general framework of designing geometrically shaped constellations for short-packet visible light communications with a peak- and an average-intensity constraints. By leveraging tools from large deviation theory, we first characterize the second-order asymptotics of the optimal constellation shaping region under aforementioned intensity constraints, which serves as a good performance measure for the best geometric shaping in finite blocklength. To further incorporate a sufficiently large coding gain and a nearly-maximum shaping gain, we construct multidimensional constellations by the nested structure of Construction B lattices, where the constellation shaping is implemented by controlling the boundary of the embedded sublattice, i.e., a strategy called coarsely shaping and finely coding. Fast algorithms for constellation mapping and demodulation are presented as well. As an illustrative example, we present an energy-efficient 24-dimensional constellation design based on the Leech lattice, whose superiority over existing constellation designs is verified by numerical results.

Index Terms—Constellation shaping, lattice codes, multidimensional constellations, short-packet transmission, visible light communication (VLC).

I. INTRODUCTION

AS a potential candidate for the next-generation wireless communication technology, visible light communication (VLC) has gained significant attention owing to integrated usage of communication and illumination, license-free deployment, inherent security, and absence of electromagnetic interference. Especially for less complexity and lower cost, intensity modulation and direct detection (IM/DD) are widely used in the VLC [1]–[3], where the IM signal is required to be real and nonnegative since the information is modulated on the optical intensity emitted from light emitting diodes (LEDs). Moreover, a peak- and/or an average-intensity constraint may be imposed on the channel input, e.g., imposing an amplitude constraint usually for safety reason or suppressing the transceiver nonlinearity [4], an average-intensity constraint for dimming control [5], or individual average-intensity constraints on multi-color LEDs for color adjustment [6]. Those

limitations lead to a fundamental difference between signaling for the IM signal in the VLC and the conventional electrical signal.

In indoor VLC scenarios, the main corruption brought by the strong background radiation and the thermal noise at the receiver photo diode (PD) can be modeled as the additive white Gaussian noise (AWGN), with which the IM/DD VLC channel is also known as *the optical intensity channel* [7]–[12]. For this reason, at the birth of the VLC, the modulation and coding schemes are simply modified versions of those for radio-frequency (RF) or fiber communications. In recent years, to improve the system throughput, extensive research efforts have been conducted to advanced signaling designs for the practical VLC systems under different constraints. In [13], [14], two-dimensional continuous-time signal spaces as well as constellation designs with respect to the corresponding discrete-time signal model are developed for the bandlimited VLC. For the VLC with a peak-intensity constraint, an efficient coded modem design is provided in [15], of which the used constellation is a variant of lattice codes based on Construction A [16, p. 29]. For the average-intensity limited VLC, probabilistically-shaped code and geometrically-shaped code are considered in [17] and [18] respectively. Signaling under dual intensity constraints is more involved due to the need of more complicated constellation shaping. In [19], a capacity-approaching non-uniform optical intensity signaling scheme under the dual intensity constraints is constructed by numerically optimizing the input distribution, while the channel coding is implemented by concatenating low density parity check (LDPC) codes with multilevel coding.

However, the above schemes either have notable performance loss due to lack of joint coding and shaping, or rely on long blocklengths for a larger coding gain or distribution mapping, and therefore, are not suitable for the short-packet VLC, which has various promising applications in industrial internet of things and vehicular communications [20]–[22]. Since short packets are utilized to carry critical control information for ultra-low latency (e.g., smaller than 0.1 ms [23]), the blocklength of used channel codes is required to be very short [24]. For the single-carrier VLC with a flat single-side bandwidth B and using a strictly bandlimited and nonnegative Nyquist pulse, the duration time of n successive symbols can be roughly evaluated by $\frac{n}{B}$ ¹. Exemplified by a commercial white LED with 5 MHz modulation bandwidth, to ensure that the user plane latency is within 0.1 ms, it is

This work is supported by Research Program of National University of Defense Technology under Grant No. ZK23-57 and ZK22-44, and the National Natural Science Foundation of China under Grant No. 62071489. Jia-Ning Guo and Jian Zhang are with National Digital Switching System Engineering and Technological Research Center, Henan Province (450000), China (e-mail: 14291003@bjtu.edu.cn, zhang_xinda@126.com). Ru-Han Chen and Xu Yang is with Sixty-Third Research Institute, National University of Defense Technology, Nanjing, China (e-mail: tx_rhc22@nudt.edu.cn, fractal_yangxu@outlook.com). Longguang Li is with Dept. Communication and Electronic Engineering, East China Normal University, Shanghai, China (e-mail: lgli@cee.ecnu.edu.cn). Jing Zhou is with Dept. Computer Science and Engineering, Shaoxing University, Shaoxing, China (e-mail: jzhou@usx.edu.cn). (Corresponding Author: Ru-Han Chen.)

¹In [25], it is proved that the maximum ISI-free symbol rate of strictly bandlimited and nonnegative continuous-time waveforms is a half of that of electrical signals.

required that the maximum blocklength can not exceed 500. Taking the packet overhead, the probability of packet loss, and potential frequency multiplexing into consideration, the actual blocklength used in the packet payload will be far less than the above value.

Motivated by the above fact, in this paper we are devoted to the signaling design for the short-packet VLC under a peak- and an average-intensity constraints². It is noted that there is no such known signaling design that approaches the Shannon limit (with respect to infinitely long blocklength) of the high signal-to-noise ratio (SNR) VLC under dual constraints at an acceptable cost, let alone characterizing the finite-blocklength limit. The main challenges in signaling for the short-packet VLC channel may come from two aspects:

- *Shaping*: For the high-SNR VLC channel, directly using the amplitude shift keying (ASK) constellation even concatenated with the best channel code will remain a constant gap to the channel capacity, for example, 1.33 dB optical SNR loss (asymptotically) in the VLC channel with limited average intensity [17], which reveals the necessity of the constellation shaping. Recently, geometric shaping has shown to be more efficient than probabilistic shaping in the short-blocklength regime, since the validity of distribution matching relies on a fairly long blocklength [27], [28]. The main challenge brought by the finite-dimensional geometric shaping is to quantitatively measure the maximum shaping gain and quickly calculate corresponding parameters in the finite-blocklength regime.
- *Coding*: In [29], the authors construct an optimally-shaped constellation based on the checkerboard lattice D_n , which limits the nominal coding gain of the constructed constellation to only 1.5 dB. To further approach the channel capacity, a more densely packing structure of constellation points should be utilized. However, how to uniquely map the message onto the signal uniformly distributed within the optimal region, and efficiently incorporate the nearly-maximum shaping gain brought by an irregular region and a large coding gain by a densely-packed lattice in a coded modulation scheme are challenging.

In this paper, for the short-packet VLC with a peak- and an average-intensity constraints, we characterize the second-order asymptotics of the maximum shaping gain (i.e., analogous to the channel dispersion [30], [31]), which touches upon the following important question in the short-packet VLC: *How much shaping gain can be attained by low-dimensional geometric shaping?* To incorporate the nearly-maximum shaping gain and a significant coding gain, we propose a general framework for signaling in finite dimensions based on Construction B lattices. The main contributions are summarized as follows:

- 1) *Second-Order Asymptotics of Optimal Shaping*: Based on the large deviation theory, we characterize the

²We would like to point out that another motivation for finite-blocklength analysis of constellation shaping comes from the fact that significant coding gains and shaping gains can be attained in relatively short blocklengths by lattice codes [16], [26].

second-order asymptotic behavior of the optimal shaping region, by which simple formulas for approximating the maximum shaping gain and the shaping parameter in the short-blocklength regime are therefore given. Numerical simulation reveals a good match of our proposed approximation even at low dimensions.

- 2) *A General Signaling Framework*: Via exploiting the algebraic structure of the Construction B lattice, we propose a novel constellation design for the short-packet VLC, which not only is compatible with a flexible choice of blocklength, but also incorporates the nearly-maximum shaping gain and a significantly larger coding gain. We further present an illustrative example by using 24-dimensional Leech lattice, which shows a performance gain of about 3 dB over the conventionally-used ASK constellation.

The remainder of this paper is organized as follows. The channel model is presented in Section II. Some preliminaries are provided in Section III. In Section IV, we characterize the second-order asymptotical properties of the optimal shaping region for the VLC under dual intensity constraints. In Section V, a general framework for the optimally-shaped constellation construction is presented. An illustrative example and relevant numerical results are given in Section VI. Section VII concludes the whole paper.

II. CHANNEL MODEL

In this paper, we consider a single-input single-output (SISO) VLC link whose channel output over n successive channel uses can be modeled by

$$\mathbf{r} = \mathbf{x} + \mathbf{z}, \quad (1)$$

where the n -dimensional real vector $\mathbf{x} = (x_1, \dots, x_n)$ denotes the instantaneously transmitted intensity signal equiprobably chosen from some multidimensional constellation \mathcal{X} , and the n -dimensional vector \mathbf{z} denotes the channel noise that modeled as the AWGN with zero mean and variance σ^2 [12].

Due to the high-SNR property of the indoor VLC channel [32] (also numerically verified in Section VI), in this paper we mainly concern with the multidimensional constellation design for intensity-modulated signals. Denote the cardinality of the constellation \mathcal{X} to be designed by $M \in \mathbb{N}_+$. Then the *normalize rate* of the constellation \mathcal{X} is $\beta = \log_2 M/n$ bits per channel use (bpcu).

Because of the nonnegativity of intensity-modulated signals, the constellation \mathcal{X} is required to satisfy

$$\mathcal{X} \subseteq \mathbb{R}_+^n,$$

where the set \mathbb{R}_+^n denotes the nonnegative orthant consisting of all nonnegative vectors in Euclidean n -space. Moreover, for the reasons of illumination control, device limitation and safety requirement in VLCs, a peak- and an average-intensity constraints are imposed on the constellation \mathcal{X} as well³

$$\max_{\mathbf{x} \in \mathcal{X}} \|\mathbf{x}\|_\infty \leq 1, \quad (2a)$$

³Without loss of generality, the maximum allowed peak intensity and the channel coefficient in the single-input single-output channel (1) can be simultaneously normalized to unity by scaling the standard deviation σ of the noise.

$$\frac{1}{nM} \sum_{\mathbf{x} \in \mathcal{X}} \sum_{i=1}^n x_i \leq \alpha, \quad (2b)$$

where the constant $\alpha \in (0, \frac{1}{2})$ denotes the ratio of the maximum allowed average intensity to the maximum allowed peak intensity.

For invariance to scaling, in this paper we define the optical signal-to-noise ratio (OSNR) as the ratio of the maximum allowed peak intensity of the input signal to the standard deviation σ of the noise, i.e.,

$$\text{OSNR} \triangleq \frac{1}{\sigma}. \quad (3)$$

Throughout the paper, we assume that perfect knowledge of channel state information is available at the receiver, which is reasonable for the quasi-static VLC channel [19]. Under this assumption, it is well-known that the error performance of the constellation \mathcal{X} at high SNR is primarily determined by the MED of the constellation \mathcal{X} as follows:

$$d_{\min}(\mathcal{X}) = \min_{\substack{\mathbf{x}_1, \mathbf{x}_2 \in \mathcal{X} \\ \mathbf{x}_1 \neq \mathbf{x}_2}} \|\mathbf{x}_1 - \mathbf{x}_2\|_2. \quad (4)$$

Therefore, the main task of this paper is to design a multi-dimensional constellation with a given normalized rate β and a MED as large as possible under the constraints (2).

III. PRELIMINARIES

For both clarity and readability of our result, in this section we first briefly introduce some concepts that are frequently used throughout the paper.

A. Construction B Lattice

An n -dimensional *lattice* is a subgroup of the Euclidean n -space with respect to the conventional vector addition operation. A *Construction B* lattice is defined as

$$\begin{aligned} H_n &= 4\mathbb{Z}^n + 2(n, n-1) + \mathcal{C}, \\ &= 2D_n + \mathcal{C} \end{aligned} \quad (5)$$

where \mathcal{C} represents an $(n, k_c, 8)$ binary linear block code and the notation $(n, n-1)$ refers to an n -dimensional parity check code, the checkerboard lattice D_n is the sublattice of \mathbb{Z}^n that consists of all points with even sum, i.e.,

$$D_n = \{(x_1, \dots, x_n) \in \mathbb{Z}^n : x_1 + \dots + x_n \text{ is even}\}.$$

As illustrated in [33], the MED of a Construction B lattice is $d_{\min}(H_n) = \sqrt{8}$.

B. Truncated Cubes

An n -dimensional *truncated cube* $\mathcal{T}_n(t)$, with the largest coordinate $t \in [0, n]$, is the intersection of a unit n -cube with an n -simplex, i.e.,

$$\mathcal{T}_n(t) \triangleq \left\{ \mathbf{x} \in [0, 1]^n : \sum_{i=1}^n x_i \leq t \right\}, \quad (6)$$

whose volume and *average first moment* are given by

$$V_n(t) = \frac{1}{n!} \sum_{k=0}^n \binom{n}{k} (-1)^k (t-k)^n \mathbf{1}_{\mathbb{R}_+}(t-k), \quad (7)$$

and

$$P_n(t) = \frac{1}{nV_n(t)} \int_{\mathcal{T}_n(t)} \|\mathbf{x}\|_1 \, d\mathbf{x} \quad (8)$$

$$= \frac{1}{n} \left(t - \frac{\sum_{k=0}^n \binom{n}{k} (-1)^k (t-k)^{n+1} \mathbf{1}_{\mathbb{R}_+}(t-k)}{V_n(t) \cdot (n+1)!} \right), \quad (9)$$

respectively, where the indicator function $\mathbf{1}_{\mathbb{R}_+}(x)$ equals one if $x \geq 0$ and otherwise zero [29].

C. Geometric Shaping

For an n -dimensional constellation \mathcal{X} chosen from the lattice Λ , say the *lattice code*, its *shaping region* \mathcal{R} is the closed region enclosing \mathcal{X} . In the following, we will present an information-theoretic definition of the shaping gain for the IM signal under a peak- and an average-intensity constraints, which is slightly different from its counterpart in coherent transmission [34].

1) *Shaping Gain*: Due to the amplitude constraint (2a), it is required that the shaping region satisfies $\mathcal{R} \subseteq [0, 1]^n$ for IM signals. In line with [15], [35], the baseline shaping region is given as the one-dimensional line segment $\mathcal{L}^\dagger = [0, 2\alpha]$. In the high-SNR regime, we utilize the n -dimensional uniform distribution $\mathbf{W}_n \sim \text{Unif}(\mathcal{R})$ and one-dimensional uniform distribution $W^\dagger \sim \text{Unif}(\mathcal{L}^\dagger)$ as the channel input distribution respectively. Then the difference between their achievable rates can be approximated by

$$\begin{aligned} & \frac{1}{n} \mathbb{I}(\mathbf{W}_n; \mathbf{W}_n + \mathbf{Z}) - \mathbb{I}(W^\dagger; W^\dagger + Z) \\ & \approx \frac{1}{n} \log(\text{vol}(\mathcal{R})) - \log(2\alpha), \end{aligned} \quad (10)$$

where $\text{vol}(\mathcal{R})$ is the n -dimensional volume of \mathcal{R} . Due to the logarithm growth of the achievable rates for AWGN channels at high SNRs, we define *the shaping gain* as

$$\text{SG}_{\text{VLC}}(\mathcal{R}) \triangleq \exp\left(\frac{1}{n} \log(\text{vol}(\mathcal{R})) - \log(2\alpha)\right) = \frac{\sqrt[n]{\text{vol}(\mathcal{R})}}{2\alpha}, \quad (11)$$

which is also compatible with another definition in [17], [29], [35] that purely based on the high-dimensional geometry.

2) *Optimal Shaping Region*: Due to the form of Eq. (11), we refer the *optimal shaping region* to the closed region \mathcal{R} with the maximized volume and satisfying corresponding constraints. For the IM signal under a peak- and an average-intensity constraints (2), finding the optimal shaping region in n -space can be formulated as the following problem:

$$\begin{aligned} \max & \quad \frac{\sqrt[n]{\text{vol}(\mathcal{R})}}{2\alpha} \\ \text{s.t.} & \quad \mathcal{R} \subseteq [0, 1]^n \\ & \quad \frac{1}{\text{vol}(\mathcal{R})} \int_{\mathcal{R}} \|\mathbf{x}\|_1 \, d\mathbf{x} \leq n\alpha, \end{aligned} \quad (12)$$

where the last inequality is a continuous version of the average-intensity constraint (2b) (see [35] for a detailed introduction of continuous approximation).

In [29], the optimal shaping region for the VLC channel under dual intensity constraints has been proved to be the family of truncated cubes. For self-containment, this result is reviewed in the following theorem.

Theorem 1. (Optimal Shaping [29]) *The optimal solution to the problem (12) is $\mathcal{T}_n(t_n^*)$ as defined in Eq. (6), where the parameter t_n^* is determined by*

$$t_n^* = \begin{cases} \mathcal{P}_n^{-1}(\alpha) & , \text{ if } \frac{1}{n+1} \leq \alpha < \frac{1}{2}, \\ (n+1)\alpha & , \text{ if } \alpha \leq \frac{1}{n+1}, \end{cases} \quad (13)$$

and $\mathcal{P}_n(\cdot)$ is given by Eq. (8). Accordingly, the maximum shaping gain in Euclidean- n space is given by

$$\overline{\text{SG}}_{\text{VLC}}(n; \alpha) = \text{SG}_{\text{VLC}}(\mathcal{T}_n(t_n^*)) = \sqrt[n]{\sqrt[n]{V_n(t_n^*)}}/2\alpha. \quad (14)$$

D. D_n Lattice Points in Truncated Cubes

Next, we review the definition of the D_n -based truncated cube developed in [29]. Let H and L be two nonnegative integers. The D_n -based truncated cube $\mathcal{TD}_n(H, 2L)$ with parameters H and L is given by

$$\mathcal{TD}_n(H, 2L) \triangleq \left\{ \mathbf{x} \in D_n \cap \{0, 1, \dots, H\}^n : \sum_{i=1}^n x_i \leq 2L \right\},$$

i.e., the subset of the checkerboard lattice consisting of all points with the ℓ_1 -norm no larger than $2L$ and amplitudes between 0 and H . We further let $\mathcal{TD}_n(H, 2L, M)$ denote the subset of $\mathcal{TD}_n(H, 2L)$, which contains M points with least ℓ_1 -norm in $\mathcal{TD}_n(H, 2L)$.

IV. OPTIMAL SHAPING IN FINITE-BLOCKLENGTH REGIMES

Commonly-used shaping methods include probabilistic shaping and geometric shaping. The former one may not be suitable for the high-SNR case due to the need of distribution matching for an input set with a large cardinality [19]. Instead, a classic coded modulation scheme, called the *lattice codes*, is widely used for bandlimited channels. The lattice code can be naturally combined with geometric shaping by the intersection of a densely-packed lattice (or its translate) and a well-chosen region in Euclidean space. In this section, based on the large deviation theory, we strength the result of geometric constellation shaping given in [29] (also see Theorem 1) through the lens of finite-blocklength analysis.

A. Finite-Blocklength Analysis of Optimal Shaping Parameter

As shown in Theorem 1, the optimal shaping parameter t_n^* should be numerically computed by the inverse of the average first moment $\mathcal{P}_n(\cdot)$ that is strictly increasing. Although the bisection algorithm is applicable for solving (13), the numerical method may become impractical as the blocklength increases, due to the presence of factorials and polynomials in (7) and (8). Additionally, lack of an analytical evaluation for the optimal shaping parameter t_n^* may hinder a concrete analysis of the maximum shaping gain. To overcome this limitation, an asymptotical analysis of the optimal shaping

region based on the large deviation theory is carried out in the following.

Without loss of generality, we let $\tau = t/n$ and accordingly $\tau_n^* = t_n^*/n$. Based on large-deviation result on the sum of independent and identically distributed (i.i.d.) random variables uniformly distributed on $[0, 1]$ (see Appendix A), we establish the asymptotics of τ_n^* in what follows.

Theorem 2. *For any given $\alpha \in (0, \frac{1}{2})$, the parameter of the optimal shaping region satisfies*

$$\tau_n^* = \alpha + \frac{1}{\mu^*} \frac{1}{n} + o\left(\frac{1}{n}\right), \quad (15)$$

where μ^* is the unique positive solution to the following equation

$$\alpha = \frac{1}{\mu} - \frac{1}{\exp(\mu) - 1}. \quad (16)$$

Proof: See Appendix B. ■

Theorem 2 shows that the optimal shaping parameter τ_n^* converges to α at a rate of $\frac{1}{\mu^*} \frac{1}{n}$, where μ^* is also the exponential decay rate of the following probability density function:

$$p_X^*(x) = \frac{\mu^*}{1 - \exp(-\mu^*)} \exp(-\mu^* x), \quad 0 \leq x \leq 1, \quad (17)$$

that maximizes the differential entropy of the input X under the support constraint $X \in [0, 1]$ and the average-intensity constraint $\mathbb{E}[X] = \alpha$ [36].

As a consequence of Theorem 2, we may approximate the shaping parameter t_n^* by $n\alpha + 1/\mu^*$, which facilitates us to determine the optimal shaping region in the application of lattice codes, rather than numerical methods.

B. Finite-Blocklength Analysis of Maximum Shaping Gain

Relying on Theorem 2, a second-order expansion of the maximum shaping gain can be obtained as follows.

Theorem 3. (Second-Order Asymptotics) *For any given $\alpha \in (0, \frac{1}{2})$, the maximum shaping gain $\overline{\text{SG}}_{\text{VLC}}(n; \alpha)$ achieved in the Euclidean- n space satisfies*

$$\log \overline{\text{SG}}_{\text{VLC}}(n; \alpha) = h_{\max}(\alpha) - \log(2\alpha) - \frac{\log(n)}{2n} + \frac{\omega_\alpha}{n} + o\left(\frac{1}{n}\right) \quad (18)$$

where $h_{\max}(\alpha)$ is the differential entropy of $p_X^*(x)$ in Eq. (17), and the constant ω_α is given by

$$\omega_\alpha = 1 - \frac{1}{2} \log \left(2\pi \left(-\mu^* + 2\alpha\mu^* + (\mu^*)^2 \alpha(1 - \alpha) \right) \right). \quad (19)$$

Proof: See Appendix C. ■

It is straightforward that we can use the second-order expansion in (18) to approximate the maximum shaping gain in finite dimensions. To the authors' best knowledge, this is the first quantitative result on measuring how much shaping gain can be obtained for the VLC in the regime of short blocklengths, which may be helpful for system design in the field. It is worth noting that the performance limit of lattice codes in the finite-blocklength regimes can be further clarified

by combining with Theorem 3 and the dispersion result of unconstrained Gaussian channel [37].

Theorem 3 also demonstrates an interesting connection between the maximum-entropy distribution and the optimal shaping region for our considered channel. It can be further proved by Theorem 3 that any marginal probability density function of the random vector uniformly distributed on $\mathcal{T}_n(t_n^*)$ converges to the maximum-entropy distribution (17), which reveals the superiority of the geometric shaping at high SNRs.

We end this subsection by relevant numerical results. In Fig. 1, we plot the absolute approximation error $t_n^* - n\alpha - 1/\mu^*$ for blocklengths n from 2 to 32, which shows a good approximation performance even at very short blocklengths.

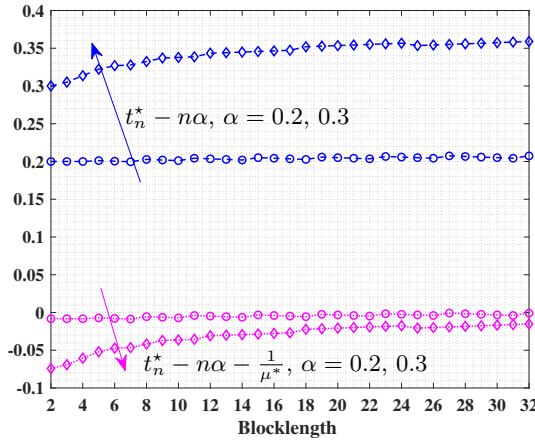


Fig. 1: The approximation error $t_n^* - n\alpha - 1/\mu^*$ versus various blocklengths n and constraint parameters α .

In Fig. 2, we plot the true maximum shaping gains and the approximated shaping gains versus various dimensions n and different intensity constraint parameters α . The results show that the true maximum shaping gain can be effectively approximated by its second-order expansion. When $n \geq 16$, the approximate error is no larger than 0.1 dB.

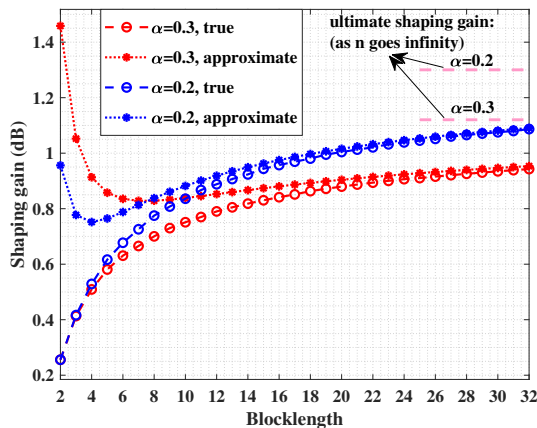


Fig. 2: True shaping gain and the second-order approximation with different constraint parameters.

Fig. 3 provides the relationship between the maximum shaping gain $\overline{\text{SG}}_{\text{VLC}}(n; \alpha)$ and the constraint parameter α in

various dimensions. It can be seen from Fig. 3 that for any $\alpha \in (0, \frac{1}{2})$, the gap between the ultimate shaping gain and the maximum shaping gain obtained in the 32-dimensional space is no larger than 0.2 dB, which indicates that most of the shaping gain can be obtained at low dimensions.

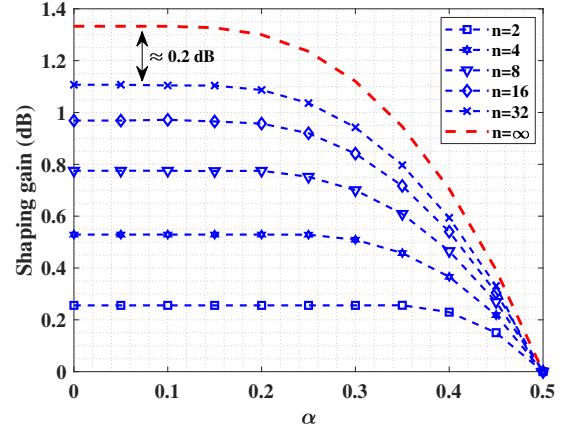


Fig. 3: The relationship between the maximum shaping gain $\overline{\text{SG}}_{\text{VLC}}(n; \alpha)$ and the constraint parameter α with different dimensions.

C. Extension to APP-Limited Quadrature Gaussian Channel

Based on the above result, we also characterize the second-order asymptotics of the maximum shaping gain for the average- and peak-power-limited (APP-limited) quadrature Gaussian channel [34], [38], whose channel output over $\frac{n}{2}$ channel uses is given by

$$\mathbf{r}_E = \mathbf{x}_E + \mathbf{z}_E, \quad (20)$$

where the $\frac{n}{2}$ -dimensional complex-valued transmitted signal $\mathbf{x}_E = (\tilde{x}_1, \dots, \tilde{x}_{\frac{n}{2}})$ is equiprobably selected from the constellation $\tilde{\mathcal{X}} \subseteq \mathbb{C}^{n/2}$ of size M . Due to the average and peak power constraints, the transmitted constellation $\tilde{\mathcal{X}}$ is required to satisfy

$$|\tilde{x}_k|^2 \leq 1, \forall k \in \{1, \dots, \frac{n}{2}\} \quad (21a)$$

$$\frac{1}{\frac{n}{2}M} \sum_{\mathbf{x}_E \in \tilde{\mathcal{X}}} \sum_{k=1}^{\frac{n}{2}} |\tilde{x}_k|^2 \leq P. \quad (21b)$$

For the APP-limited quadrature Gaussian channel, the shaping gain of a given closed region \mathcal{R} of the corresponding Euclidean n -space is defined as

$$\text{SG}_E(\mathcal{R}) = \frac{\text{PAPR}(\mathcal{R})}{3}, \quad (22)$$

where the quantity 3 is the peak-to-average-power ratio (PAPR) of the n -cube [34]. For simplicity, the maximum shaping gain within the blocklength $\frac{n}{2}$ of the APP-limited quadrature Gaussian channel is denoted by $\overline{\text{SG}}_E(\frac{n}{2}; P)$, which is achieved by the n -dimensional real-valued truncated poly-disc (see [34] for a detailed description). Combining [34, (9)] and Theorem 3, we can readily derive the second-order

asymptotics of the maximum shaping gain for the APP-limited quadrature Gaussian channel in the following corollary, which may be of independent interests.

Corollary 1. *The maximum shaping gain of the APP-limited quadrature Gaussian channel satisfies*

$$\begin{aligned} & \overline{\text{SG}}_{\text{E}}\left(\frac{n}{2}; \text{P}\right) \\ &= \frac{\pi}{3} \overline{\text{SG}}_{\text{VLC}}(n; \text{P}) \\ &= 0.200 + \text{h}_{\text{max}}(\text{P}) - \log(2\text{P}) - \frac{\log(n)}{2n} \\ & \quad + \frac{\omega_{\text{P}}}{n} + o\left(\frac{1}{n}\right) \quad (\text{in dB}). \end{aligned} \quad (23)$$

We especially point out that, by letting $\text{P} \rightarrow 0$ and $n \rightarrow +\infty$, Corollary 1 coincides with the well-known results that the ultimate shaping gain (with respect to OSNR) for the VLC channel with only an average-intensity constraint is 1.33 dB (see [17]), while that (with respect to electrical SNR) for the AWGN channel with only an average-power constraint is 1.53 dB.

V. OPTIMALLY-SHAPED CONSTELLATION BASED ON CONSTRUCTION B LATTICES

In Section IV, we derive the second-order asymptotics of the optimal shaping parameter t_n^* and the maximum shaping gain $\overline{\text{SG}}_{\text{VLC}}(n; \alpha)$ for the VLC channel under the dual intensity constraints, which answers the question that how much shaping gain can be achieved by finite-dimensional geometric shaping. In order to improve the coding gain, one approach is to employ an inequidistant ASK constellation in conjunction with powerful channel codes like LDPC codes. However, it may not be suitable for indoor VLC scenarios due to the need of distribution matching and time-consuming iterative decoding algorithms.

Therefore, in this section, we propose a general signaling framework by constructing geometrically-shaped constellations, which has flexible normalized rates, low implementation complexity, and a substantial OSNR gain as compared with existing schemes.

A. Basic Idea of Constructing Geometrically-Shaped Constellations

1) *Denser Packing via Construction B Lattice:* It is noted that the most of the ultimate shaping gain $\overline{\text{SG}}_{\text{VLC}}(+\infty; \alpha)$ can be achieved in finite dimensions (as illustrated in Fig. 3), while there is still much room for further improvement of the coding gain. In [29], both the shaping and the coding of the truncated cubic constellation (TCC) are carried out by the checkerboard lattice D_n , of which a nominal coding gain of 1.5 dB (with respect to the OSNR definition (3)) is attained as compared with the ASK constellation.

To address the limitation of the D_n lattice on the coding gain of the TCC, we leverage the densely-packing structure of the Construction B lattice, or more generally, the union of cosets of the Construction B lattice

$$\Lambda_n = \bigcup_{\mathbf{a} \in \mathcal{A}} (2H_n + \mathbf{a}), \quad (24)$$

where \mathcal{A} is the union of coset representatives. It has been found that many dense lattice packings in low dimensions can be constructed by translating a Construction B lattice, such as E_8 lattice, BW_{16} lattice, and Leech lattice [33]. The good choice of \mathcal{A} varies greatly with the blocklength n , and hence, is not specified here.

2) *Coarsely Shaping and Finely Coding:* To integrate the coding gain of the finitely-shifted Construction B lattice and the nearly-maximum shaping gain in the constellation construction, a natural way is selecting M points from the lattice Λ_n within the optimal shaping region $\mathcal{F}_n(t_n^*)$ (scaling by an appropriate factor). However, directly enumerating M points from the intersection of a delicately-constructed lattice Λ_n with a nontrivial Voronoi cell and the optimal shaping region is challenging, and a look-up table may lead to an exponential growth of the computation complexity and the storage complexity as the normalized rate β increases.

To address this issue, resorting to the idea of *coarsely shaping and finely coding* and the structure of Construction B lattices, we construct the multidimensional constellation with a near-optimal shape by assigning the task of constellation shaping to a sublattice of the embedded Construction B lattice.

For better readability, here we briefly illustrate the basic idea of coarsely shaping and finely coding by a two-dimensional example in Fig. 4. Suppose we select M points from the D_2 lattice, whose boundary is required to look like a given truncated cube. Note that D_2 can be represented in a Construction A form

$$D_2 = 2\mathbb{Z}^2 + C_2, \quad (25)$$

where the set $C_2 = \{\mathbf{0}_2, \mathbf{1}_2\}$. Then a simple construction method is first selecting $M/2$ $2\mathbb{Z}^2$ points from the desired truncated cube (see blue small circles in Fig. 4) and then translating those points by the vector $\mathbf{1}_2 \in C_2$ (see magenta small diamonds in Fig. 4). It can be seen that the overall boundary almost maintains the desired shape, say coarsely shaping, while simultaneously all points are selected from D_2 lattice which determines the MED of the constructed constellation, say finely coding.

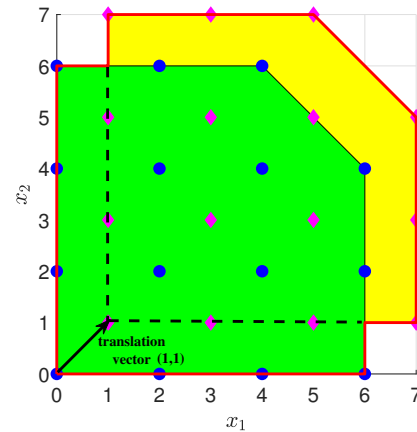


Fig. 4: Coarsely shaping and finely coding for selecting D_2 points from a truncated cube.

B. Framework of Constellation Construction

Combining the construction (5) of H_n , and analogue to the above two-dimensional example, our constellation construction is formally given in what follows:

$$\mathcal{L}_n = \bigcup_{\mathbf{a} \in \mathcal{A}} \underbrace{4\mathcal{D}_{\text{shape}}}_{\text{shaping part}} + \underbrace{2\mathcal{C} + \mathbf{a}}_{\text{coding part}}, \quad (26)$$

where the shaping set $\mathcal{D}_{\text{shape}}$ is chosen from the D_n lattice and used to control the overall shape of \mathcal{L}_n . It is clear that the so-constructed constellation \mathcal{L}_n is obtained via translating (at a small scale) $\mathcal{D}_{\text{shape}}$ by the quotient set $[\Lambda_n/4D_n]$. In the following, three crucial issues in constructing \mathcal{L}_n are clarified in detail.

1) *Choice of $\mathcal{D}_{\text{shape}}$* : Assume that there are 2^{k_a} elements in the set \mathcal{A} . Let the constants $k_s = n\beta - k_c - k_a$ and $M_s = 2^{k_s}$. Therefore, to get a near-maximum shaping gain, the shaping set $\mathcal{D}_{\text{shape}}$ is required to contain M_s D_n lattice points within the optimal shaping region $\mathcal{T}_n(t_n^*)$ (with appropriate scaling), which is exactly the set $\mathcal{D}_n(H^*, 2L^*, M_s)$, where the involved parameters H^* and L^* can be uniquely determined by using Algorithm 1 in [29] for constructing TCCs.

2) *Fast Constellation Mapping*: It is recognized that a constellation addressing algorithm that quickly maps the message onto the desired constellation point $\boldsymbol{\lambda} \in \mathcal{L}_n$ is needed to reduce the implementation complexity of geometric shaping. According to the form of the construction (26), we shall divide the message into three parts, which are mapped onto the shape set $\mathcal{D}_{\text{shape}}$, the component $(n, k_c, 8)$ code \mathcal{C} , and the set \mathcal{A} of coset representatives, respectively. The last two mappings are straightforward and very fast, while fortunately, the mapping onto $\mathcal{D}_{\text{shape}}$ can be efficiently solved by the FFT-assisted decomposable shell mapping (FDSM) in [29] at the computational cost approximately linear with the blocklength.

For clarity, we summarize the detailed procedures that map a binary sequence \mathbf{b} onto the constellation point $\boldsymbol{\lambda} \in \mathcal{L}_n$ in the following.

- *Step 1: Data partition*. Let $\mathbf{b} \in \mathbb{F}_2^k$ be a length- k binary sequence, where $k = n\beta$. Then divide \mathbf{b} into three parts $\mathbf{b}_s = (b_1, \dots, b_{k_s})$, $\mathbf{b}_c = (b_{k_s+1}, \dots, b_{k_s+k_c})$, and $\mathbf{b}_a = (b_{k_s+k_c+1}, \dots, b_k)$.
- *Step 2: Coarsely shaping*. Map the length- k_s binary sequence \mathbf{b}_s onto some n -dimensional lattice point $\mathbf{d} = (d_1, \dots, d_n) \in \mathcal{D}_n(H^*, 2L^*, M_s)$ by the FDSM algorithm [29, Algorithm 2].
- *Step 3: Block coding*. Map the length- k_c binary sequence \mathbf{b}_c onto some codeword $\mathbf{c} = (c_1, \dots, c_n) \in \mathcal{C}$.
- *Step 4: Coset mapping*. Map the length- k_a binary sequence \mathbf{b}_a onto some coset representative $\mathbf{a} \in \mathcal{A}$ via an enumeration approach. Then the desired constellation point is obtained as $\boldsymbol{\lambda} = 4\mathbf{d} + 2\mathbf{c} + \mathbf{a}$.

3) *Constellation Scaling*: For simplicity, in the above we construct the desired constellation based an unnormalized Construction B lattice, which should be scaled to meet the input constraints (2). Here we will briefly discuss how to evaluate the scaling factor $\kappa \in \mathbb{R}_+$.

Note that the peak value of the proposed constellation \mathcal{L}_n is given by

$$\max_{\boldsymbol{\lambda} \in \mathcal{L}_n} \|\boldsymbol{\lambda}\|_\infty \quad (27)$$

$$\begin{aligned} &= \max_{\substack{\mathbf{d} \in \mathcal{D}_n(H^*, 2L^*, M_s) \\ \mathbf{c} \in \mathcal{C}, \mathbf{a} \in \mathcal{A}}} \|4\mathbf{d} + 2\mathbf{c} + \mathbf{a}\|_\infty \\ &= 4H^* + 2 + \max_{\mathbf{a} \in \mathcal{A}} \|\mathbf{a}\|_\infty. \end{aligned} \quad (28)$$

Similarly, the average intensity of \mathcal{L}_n is given by

$$\begin{aligned} &\frac{1}{nM} \sum_{\mathbf{x} \in \mathcal{L}_n} \|\mathbf{x}\|_1 \\ &= \frac{1}{nM} \sum_{\substack{\mathbf{d} \in \mathcal{D}_{24}(H^*, 2L^*, M_s) \\ \mathbf{c} \in \mathcal{C}, \mathbf{a} \in \mathcal{A}}} \|4\mathbf{d} + 2\mathbf{c} + \mathbf{a}\|_1 \\ &= \frac{4}{M_s} \sum_{\mathbf{d} \in \mathcal{D}_n(H^*, 2L^*, M_s)} \|\mathbf{d}\|_1 + 1 + \frac{\sum_{\mathbf{a} \in \mathcal{A}} \|\mathbf{a}\|_1}{2^{k_a}}, \end{aligned} \quad (30)$$

where Eq. (30) follows from the fact that the uniformity of any linear code.

Thus, to satisfy the intensity constraints (2), the scaling factor κ should be set as

$$\kappa = 1 / \max \left\{ \max_{\boldsymbol{\lambda} \in \mathcal{L}_n} \|\boldsymbol{\lambda}\|_\infty, \frac{1}{nM} \sum_{\boldsymbol{\lambda} \in \mathcal{L}_n} \|\boldsymbol{\lambda}\|_1 / \alpha \right\}. \quad (31)$$

We would like to point that, for simplicity of implementation, the maximum coordinate H^* and the average ℓ_1 -norm of $\mathcal{D}_n(H^*, 2L^*, M_s)$ can be roughly estimated by using the optimal shaping region $\mathcal{T}_n(t_n^*)$ via continuous approximation (or say, the Minkowski-Hlawka theorem [39, Thm. 1]).

C. Demodulation Algorithm

With perfect CSI at the receiver, the maximum likelihood (ML) demodulator performs the minimum-distance detection as

$$\hat{\boldsymbol{\lambda}} = \underset{\boldsymbol{\lambda} \in \mathcal{L}_n}{\operatorname{argmin}} \|\boldsymbol{\lambda} - \mathbf{r}/\kappa\|_2. \quad (32)$$

For simplicity, we let $\mathbf{y} = \mathbf{r}/\kappa$. However, for the used constellation \mathcal{L}_n with a finite cardinality, an irregular boundary, and a complicated multi-layer construction in Eq. (26), the ML demodulation is not feasible in practice due to the complexity limitation. For this reason, we resort to a bounded-distance decoding algorithm for Construction B lattices, which was proposed in [33] and shown to have near-optimal performance with respect to the symbol error probability.

1) *Bounded-Distance Decoding*: For any given vector $\mathbf{y} \in \mathbb{R}^n$ and a Construction B lattice H_n , the bounded-distance decoding algorithm [33, Algorithm 2] outputs the point \mathbf{h} from H_n (i.e., infinite constellation) that is closest to \mathbf{y} if $\|\mathbf{h} - \mathbf{y}\| \leq d_{\min}(H_n)/2 = \sqrt{2}$, i.e., performs as optimal algorithms within a ball of certain radius. For self-containment, we shall review the main idea of this algorithm in what follows.

It is clear that

$$H_n \subseteq U_n = 2\mathbb{Z}^n + \mathcal{C}, \quad (33)$$

where U_n is a Construction A lattice which is obtained by replacing the single-parity code in constructing H_n to $\{0, 1\}^n$,

where the quotient set $[U_n/H_n] = \{\mathbf{0}_n, (\mathbf{0}_m, 2, \mathbf{0}_{n-m-1})\}$ with an arbitrary integer m ranging from 0 to $n - 1$. The aforementioned algorithm first searches the closest point from U_n , which can be quickly solved by combining integer forcing and soft decoding of the binary linear block code \mathcal{C} due to the property of Construction A lattices [40]. Then the algorithm translates such the closest point from U_n in some way to ensure that the final output point is selected from the sublattice H_n .

2) *Demodulation Procedure*: Motivated by the above fact, the demodulation of our proposed constellation \mathcal{L}_n can be implemented via a lattice decoding approach. The detailed procedures are summarized in the following.

- *Step 1: Closest point search in U_n* [40]. For any $\mathbf{a} \in \mathcal{A}$, let $\mathbf{w}(\mathbf{a}) = (\mathbf{y} - \mathbf{a})/2$. Let $\hat{\mathbf{u}}(\mathbf{a}) = 2\hat{\mathbf{z}} + \hat{\mathbf{c}}$ be the closest point in U_n to $\mathbf{w}(\mathbf{a})$, where the integer component $\hat{\mathbf{z}}$ and the binary linear block codeword $\hat{\mathbf{c}}$ are computed by using the decoding algorithm for Construction A lattices [40, p. 450], along with the soft decoding algorithm for the binary linear block code \mathcal{C} .
- *Step 2: Bounded-distance decoding in H_n* [33]. Let $\hat{\mathbf{h}}(\mathbf{a}) = \hat{\mathbf{u}}(\mathbf{a})$. If the integer component $\hat{\mathbf{z}}$ has an even sum, we directly output $\hat{\mathbf{h}}(\mathbf{a})$ as the bounded-distance decoding result for H_n . Otherwise, search the smallest index i satisfying

$$i = \operatorname{argmax}_{j \in \{1, 2, \dots, n\}} |w_j(\mathbf{a}) - \hat{u}_j(\mathbf{a})|, \quad (34)$$

translate $\hat{\mathbf{h}}(\mathbf{a})$ by

$$\hat{h}_i(\mathbf{a}) = \begin{cases} \hat{u}_i(\mathbf{a}) + 2, & \text{if } w_i(\mathbf{a}) \geq \hat{u}_i(\mathbf{a}); \\ \hat{u}_i(\mathbf{a}) - 2, & \text{if } w_i(\mathbf{a}) < \hat{u}_i(\mathbf{a}). \end{cases} \quad (35)$$

and then output the modified $\hat{\mathbf{h}}(\mathbf{a})$.

- *Step 3: Bounded-distance decoding in Λ_n* [33]. For each $\mathbf{a} \in \mathcal{A}$, compute Euclidean distances between $2\hat{\mathbf{h}}(\mathbf{a}) + \mathbf{a}$ and \mathbf{y} , and then select the closest one to \mathbf{y} as the demodulator output $\hat{\lambda}$.

Note that the constellation demapping of the demodulator output $\hat{\lambda}$ onto the binary sequence is a simple inverse transform of the constellation mapping, and therefore omitted.

VI. DESIGN EXAMPLES AND NUMERICAL RESULTS

In this section, we present an illustrative example of our proposed constellation design framework, and then numerically verify its superiority as compared with the existing schemes.

A. Optimally-Shaped Leech Constellation

In this subsection, we show a concrete implementation of our proposed constellation design, by which an energy-efficient 24-dimensional constellation for our considered channel is designed. Note that the densest packing in 24-dimensional Euclidean space has been proved to be the Leech lattice Λ_{24} [41], by which an extra nominal coding gain of 3 dB (effective coding gain of 2 dB) may be attained. A method of constructing the Leech lattice via Construction B is introduced in the following.

1) *Leech Lattice via Construction B*: Denote the Leech half-lattice by H_{24} , which can be constructed via Construction B as follows:

$$H_{24} \triangleq 4\mathbb{Z}^{24} + 2(24, 23) + G_{24} = 2D_{24} + G_{24}, \quad (36)$$

where the notation $(24, 23)$ refers to the 24-dimensional parity check codes, and G_{24} is the $(24, 12, 8)$ Golay code. In [40], [42], [43], a method of constructing the Leech lattice Λ_{24} is presented by translating H_{24} as

$$\Lambda_{24} = 2H_{24} \cup (2H_{24} + \boldsymbol{\xi}), \quad (37)$$

where the 24-dimensional translation vector $\boldsymbol{\xi} = (-3, \mathbf{1}_{23}) \in \mathbb{R}^{24}$.

2) *Construction Procedures*: In line with Section V-B, an optimally-shaped Leech constellation (OSLC) can be constructed in what follows.

Combining Eqs. (26) and (36), we define

$$\mathcal{H}_{24} = 2\mathcal{D}_{\text{shape}} + G_{24}, \quad (38)$$

where the shaping set $\mathcal{D}_{\text{shape}} = \mathcal{D}_{24}(H^*, 2L^*, 2^{24\beta-13}) \subseteq D_{24}$ is obtained as described in Section V-B1. To ensure the nonnegativity of the constructed constellation, a slight modification to the next translation operation is needed. Concretely speaking, we construct the OSLC as

$$\mathcal{L}_{24} = \bigcup_{\mathbf{h} \in \mathcal{H}_{24}} \bigcup_{\mathbf{b} \in \{0_{24}, \tilde{\boldsymbol{\xi}}(\mathbf{h})\}} 2\mathbf{h} + \mathbf{b}, \quad (39)$$

where the modified translation vector $\tilde{\boldsymbol{\xi}}(\mathbf{h})$ is given by

$$\tilde{\boldsymbol{\xi}}(\mathbf{h}) = \begin{cases} (5, \mathbf{1}_{23}) & , 2h_1 \bmod 8 < 3, \\ (-3, \mathbf{1}_{23}) & , 2h_1 \bmod 8 > 3, \end{cases} \quad (40)$$

and the quantity h_1 denotes the first coordinate of $\mathbf{h} \in \mathcal{H}_{24}$. It can be easily verified that, after the above modified translation, so-constructed constellation still lies in the nonnegative orthant and has a cardinality of M . For a clearer illustration, we plot procedures of constellation mapping of the OSLC \mathcal{L}_{24} in Fig. 5.

B. Error Performance of \mathcal{L}_{24}

In this subsection, to verify the advantages of our proposed OSLC, we present numerical results on its symbol error rates (SERs). As benchmark schemes, the cubic constellation (i.e., the 24-times Cartesian product of an ASK constellation) and the D_{24} -based TCC proposed in [29] are considered as well.

1) *AWGN Channels*: We first consider the SER performance of the above three constellations over the AWGN channel. By varying the normalized rate β from 2 bpcu to 5 bpcu, Fig. 6 plots their SER curves with $\alpha = 0.2$, while Fig. 7 plots those curves in the case of $\alpha = 0.3$. It can be seen that the OSLC significantly outperforms two benchmark schemes when the normalized rate $\beta = 4$ and 5. In the case of $\alpha = 0.2$ and $\beta = 5$, the OSLC has OSNR gains of 3 dB and 0.9 dB at a target SER 10^{-5} , as compared to the cubic constellation and the TCC, respectively, while OSNR gains of 2.8 dB and 0.9 dB can be observed when $\alpha = 0.3$. It is noted that there is a 0.2 dB difference in the OSNR gains compared with the

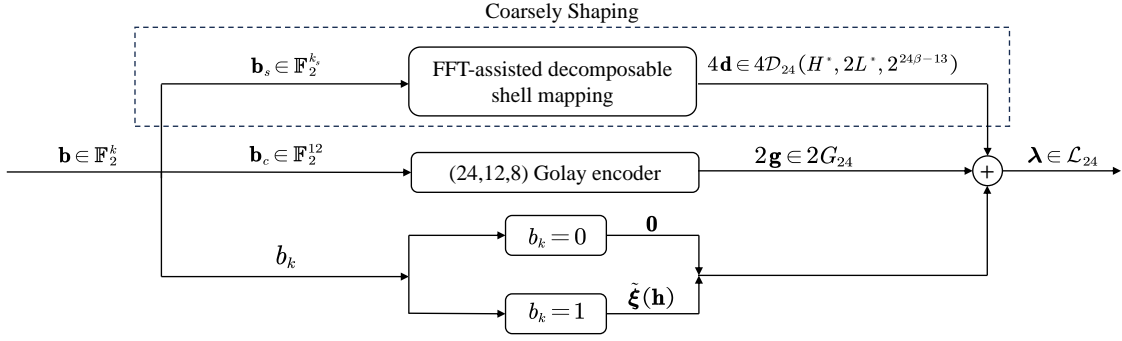
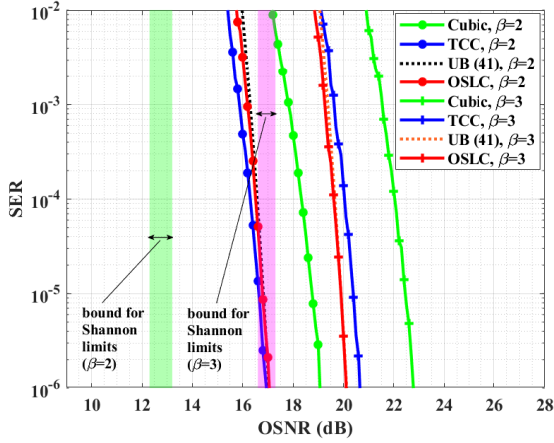
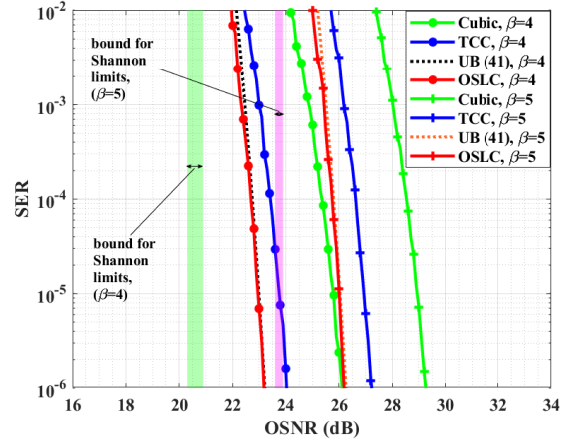
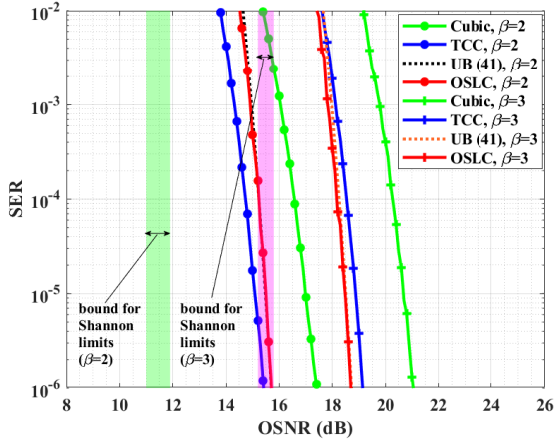
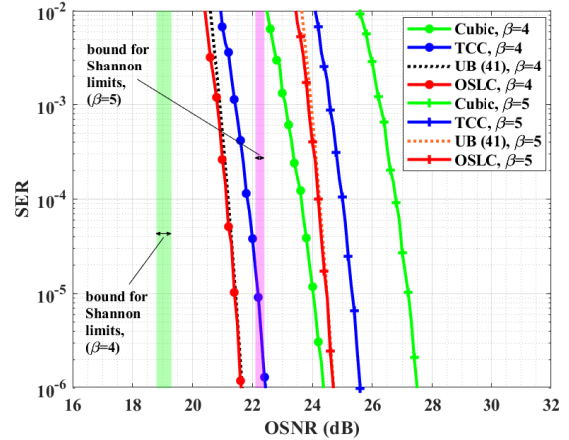


Fig. 5: Constellation mapping for the OSLC.

(a) The SER curves of the OSLC scheme and the benchmarks with $\alpha = 0.2$ when $\beta = 2$ bpcu and 3 bpcu.(b) The SER curves of the OSLC scheme and the benchmarks with $\alpha = 0.2$ when $\beta = 4$ bpcu and 5 bpcu.Fig. 6: The SER curves of the OSLC scheme and the benchmarks with $\alpha = 0.2$.(a) The SER curves of the OSLC scheme and the benchmarks with $\alpha = 0.3$ when $\beta = 2$ bpcu and 3 bpcu.(b) The SER curves of the OSLC scheme and the benchmarks with $\alpha = 0.3$ when $\beta = 4$ bpcu and 5 bpcu.Fig. 7: The SER curves of the OSLC scheme and the benchmarks with $\alpha = 0.3$.

cubic constellation (i.e., without constellation shaping), which is consistent with our result on the second-order asymptotics of the maximum shaping gain (see Fig. 3). As the normalized

rate β decreases, the performance advantage of the OSLC over the TCC diminishes. From Fig. 6(a) and Fig. 7(a), it can be observed that the SERs of the TCC are close to those of the

OSLC at $\beta = 3$, and at $\beta = 2$ the TCC slightly outperforms the OSLC. The main reasons for this reduction in OSNR gains may come from three aspects: 1) by using the coarsely shaping and finely coding strategy, only a small part of the message sequence is used for geometrically shaping the OSLC when β is small, which results to a shaping region of \mathcal{L}_{24} that may be far less like the optimal shaping region; 2) the densely-packed structure (39) of the OSLC \mathcal{L}_{24} may be broken in the regime of a small cardinality; 3) the lattice decoding algorithm leads to performance loss as compared with the ML decoding, especially when the cardinality of the lattice code is relatively small.

It is also seen that the SERs of the OSLC can be well evaluated by

$$P_{e,UB} = N_A Q(\kappa d_{\min}/2\sigma), \quad (41)$$

i.e., the union bound (UB) on the error probability for the ML decoding of the Leech lattice Λ_{24} , where $Q(u) \triangleq \frac{1}{\sqrt{2\pi}} \int_u^\infty e^{-y^2/2} dy$ is the Gaussian Q-function, and $N_A = 196560$ and $d_{\min} = 4\sqrt{2}$ represent the kissing number and the MED of the Leech lattice Λ_{24} , respectively [40]. This observation shows that the error performance of the bounded-distance algorithm used in our demodulator is very close to that of the best lattice decoding algorithm. In practical implementation, the UB (41) can be used for predicting the error performance of the OSLC.

We also evaluate the performance gap between the OSLC and the Shannon limit. Note that there is no closed-form formula for the exact channel capacity of our considered VLC channel. Hence, we use the capacity upper and lower bounds given in [19], [36] and plot those bounds in Figs. 6 and 7 by semi-transparent strips. From Figs. 6(b) and 7(b), it can be seen that, the gap between the OSLC and the ultimate limit are within 2.5 dB in the high-SNR regimes, which is mainly caused by the fundamental backoff due to finite blocklength.

C. Indoor VLC Scenario

We particularly provide a glimpse of the error performance of the OSLC in an indoor VLC scenario, where a 4 m × 4 m × 3 m room with 4 LED lamps of the same specification and a single receiver PD is considered. We assume that the LED lamps are installed on the ceiling and equipped with 7 × 7 LED array, and one receiver PD is located on the plane at height of 0.6m. Other parameters of the LED transmitters and the PD receiver are listed in Tables I and II, respectively. As pointed in [44], if those LED lamps are required to have identical brightness, the considered MISO VLC channel is equivalent to a scalar VLC channel via spatial repetition coding, and our proposed constellation can be readily used.

Denote the drive current of all LED chips by I . After removing the DC component and spatial repetition coding, the equivalent scalar VLC channel is given by

$$R = \sum_{q=1}^4 \sum_{j=1}^{49} s \cdot h_{qj} \cdot \gamma \cdot (I - I_{\min}) + Z, \quad (42)$$

where the channel coefficients h_{qj} are computed by Lambertian's model as in [32]. With the same treatment in [45], the variance of the AWGN σ^2 is approximated by

$$\sigma^2 = 2q_e B \left(\sum_{q=1}^4 \sum_{j=1}^{49} s \cdot h_{qj} \cdot \gamma \cdot \mathbb{E}[I] + I_{bg} I_2 \right), \quad (43)$$

where the quantity q_e denotes the electronic charge. It is straightforward that $I \in [0.4, 0.6]$. Let $X = (I - I_{\min}) / (I_{\max} - I_{\min})$ and the dimming factor $\alpha = (\mathbb{E}[I] - I_{\min}) / (I_{\max} - I_{\min})$, and then, after an appropriate linear transform, the model (42) can be rewritten as

$$R = X + \sigma^2 / \left(0.2s \cdot \gamma \cdot \left(\sum_{q=1}^4 \sum_{j=1}^{49} h_{qj} \right) \right), \quad (44)$$

where the block code \mathcal{X} with blocklength n for the new input X is subject to the constraints (2).

We first plot the simulated OSNR for the considered scenario in Fig. 8, from which it can be seen that the received OSNRs are about 25 – 26 dB. In the last subsection, numerical results for the AWGN channel have indicated that high normalized rates can be achieved at those high SNRs. Table III lists the average SER of our proposed scheme and the benchmarks with the normalized rate $\beta = 5$ for the considered indoor channel, where the receiver PD is randomly located at (X_P, Y_P) with two coordinates X_P and Y_P independently and uniformly distributed on the interval $[-4, 4]$. Numerical results also verify the performance advantage of our schemes over others in the indoor VLC application.

TABLE I: Transmitter Parameters

LED lamp coordinates	$(\pm 1.6, \pm 1.6, 3)$ [m]
Minimum drive current I_{\min}	0.4 [A]
Maximum drive current I_{\max}	0.6 [A]
Semi-angle at half power	60°
Interval of the LED array	1 [cm]
O/E conversion efficiency of LED γ	0.45 [W/A]

TABLE II: Receiver Parameters

Physical area of PD	1 [cm ²]
Gain of optical filter	1
Refractive index of the lens at PD	1.5
Responsivity of PD s	0.4 [A/W]
Field of view (FOV)	60°
System bandwidth B	10 [MHz]
Noise bandwidth factor I_2	0.562
Background current I_{bg}	100 [μ A]

VII. CONCLUSION

In this paper, a general framework for signaling over the short-packet VLC channel with a peak- and an average-intensity constraints is proposed. It mainly consists of

TABLE III: Average SER for the indoor VLC system.

Average SER \ Parameter α	0.2	0.3
Scheme		
Cubic constellation	0.3004	0.0196
TCC	0.0241	3.727×10^{-6}
OSLC	7.501×10^{-4}	$\ll 10^{-6}$

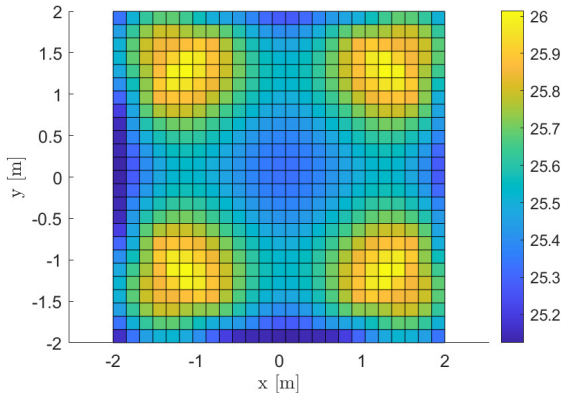


Fig. 8: The simulation of OSNR for the 4m×4m×3m room.

nite blocklength analysis of geometric shaping and an elaborated method of constructing geometrically-shaped multi-dimensional constellations. Additionally, we present a 24-dimensional constellation design based on the Leech lattice as an illustrative example, which shows a significant OSNR gain as compared with existing schemes.

ACKNOWLEDGEMENT

This work is supported by the National Natural Science Foundation of China (NSFC) under Grant (62071489).

APPENDIX A

LARGE DEVIATION OF SUM OF INDEPENDENT RANDOM VARIABLES UNIFORMLY DISTRIBUTED ON $[0, 1]$

Let the random variable U be uniformly distributed on $[0, 1]$. For $s > 0$, the moment-generating function of U is

$$M(s) \triangleq \mathbb{E}[\exp(sU)] = \frac{\exp(s) - 1}{s},$$

and we define

$$K(s) \triangleq \frac{M'(s)}{M(s)} = \frac{\exp(s)}{\exp(s) - 1} - \frac{1}{s}.$$

It is clear that $K(s)$ is monotone increasing and satisfies $K(0^+) = \frac{1}{2}$ and $K(+\infty) = 1$. Then, we let s_x denote the unique solution to the equation

$$K(s_x) = x, \quad (45)$$

where $x \in [\frac{1}{2}, 1]$. Specially, an immediate consequence of (16) is

$$\mu^* = s_{1-\alpha}. \quad (46)$$

Clearly, the solution s_x increases with x . Then, for $x \in [\frac{1}{2}, 1]$, we define

$$L(x) \triangleq \log(M(s_x)) - xs_x,$$

and

$$D(x) \triangleq s_x \sqrt{K'(s_x)} = \sqrt{\frac{-s_x^2 \cdot \exp(s_x)}{(\exp(s_x) - 1)^2} + 1}.$$

It can be easily verified both $L(x)$ and $D(x)$ are smooth. Then, by computing high-order derivatives of $D(x)$, we can show that $D(x)$ is bounded and non-decreasing with x . Also, we note that

$$L'(x) = \left(\frac{M'(s_x)}{M(s_x)} - x \right) \cdot \frac{ds_x}{dx} - s_x \quad (47)$$

$$= (K(s_x) - x) \cdot \frac{ds_x}{dx} - s_x \quad (48)$$

$$= -s_x. \quad (49)$$

Since s_x is increasing as x increases, the function $L(x)$ is concave and thus satisfies

$$L(x) \leq L(1 - \tau) - s_{1-\tau}(x - (1 - \tau)). \quad (50)$$

for any x and τ in $[\frac{1}{2}, 1]$.

Denote the tail probability of the sample mean $\bar{U}_n = \frac{1}{n} \sum_{i=1}^n U_i$ by $G_n(x) = \mathbb{P}\{\bar{U}_n \geq x\}$. Based on Theorem 1 in [46], the sequence of functions

$$G_n(x) = \frac{\exp(nL(x))}{\sqrt{2\pi nD(x)}}(1 + o(1)) \quad (51)$$

as $n \rightarrow \infty$ uniformly in x in the closed interval $[\frac{1}{2} + \epsilon, 1 - \epsilon]$, where ϵ is an arbitrarily positive constant.

APPENDIX B

PROOF OF THEOREM 2

The average first moment of $\mathcal{T}_n(n\tau)$ can be alternatively expressed by the conditional expectation of the Irwin-Hall distribution as follows

$$P_n(n\tau) = \frac{1}{n} \sum_{i=1}^n \mathbb{E} \left[U_i \mid \sum_{i=1}^n U_i \leq n\tau \right] \quad (52)$$

$$= \mathbb{E}[\bar{U}_n \mid \bar{U}_n \leq \tau] \quad (53)$$

$$= 1 - \mathbb{E}[\bar{U}_n \mid \bar{U}_n \geq 1 - \tau]. \quad (54)$$

$$(55)$$

Remind that the tail probability $G_n(x) = \mathbb{P}\{\bar{U}_n \geq x\}$. Then, it is straightforward that

$$P_n(n\tau) = 1 + \frac{\int_{1-\tau}^1 x dG_n}{G_n(1-\tau)} \quad (56)$$

$$= \tau - \int_{1-\tau}^1 \frac{G_n(x)}{G_n(1-\tau)} dx. \quad (57)$$

The first-moment condition (13) immediately shows that

$$\alpha = \tau_n^* - \int_{1-\tau_n^*}^1 \frac{G_n(x)}{G_n(1-\tau_n^*)} dx. \quad (58)$$

It is clear that $\tau_n^* \geq \alpha$ for any n . Next, we will prove that

$$\lim_{n \rightarrow \infty} n(\tau_n^* - \alpha) = \frac{1}{s_{1-\alpha}}. \quad (59)$$

Note that $\tau \geq \alpha$ and $P_n(1) = \frac{1}{2}$. For any $\tau \in (0, 1)$, there exists a positive (and possibly arbitrarily small) constant ϵ such that $1 - \tau + 2\epsilon \leq 1$. Then we note that

$$0 \leq \int_{1-\tau}^1 \frac{G_n(x)}{G_n(1-\tau)} dx \leq 2\epsilon + \int_{1-\tau+\epsilon}^{1-\epsilon} \frac{G_n(x)}{G_n(1-\tau)} dx. \quad (60)$$

Due to the uniform convergence of $G_n(x)$, we can rewrite

$$\begin{aligned} & \int_{1-\tau+\epsilon}^{1-\epsilon} G_n(x) dx \\ &= \int_{1-\tau+\epsilon}^{1-\epsilon} \frac{\exp(nL(x))}{\sqrt{2\pi n}D(x)} (1+o(1)) dx \\ &\leq \int_{1-\tau+\epsilon}^{1-\epsilon} \frac{\exp(n(L(1-\tau) - s_{1-\tau}(x - (1-\tau))))}{\sqrt{2\pi n}D(1-\tau)} (1+o(1)) dx \\ &\leq \frac{1}{s_{1-\tau}} G_n(1-\tau) \left(\frac{1}{n} + o\left(\frac{1}{n}\right) \right) \end{aligned} \quad (61)$$

Immediately, we have $\tau_n^* = \alpha + o(1)$. Note that

$$\begin{aligned} & n(\tau_n^* - \alpha) \\ &= n \int_{1-\tau_n^*}^1 \frac{G_n(x)}{G_n(1-\tau_n^*)} dx \end{aligned} \quad (62)$$

$$\leq n \left(\int_{1-\tau_n^*}^{1-\epsilon} \frac{G_n(x)}{G_n(1-\tau_n^*)} dx + \epsilon \frac{G_n(1-\epsilon)}{G_n(1-\tau_n^*)} \right) \quad (63)$$

$$= \frac{1}{s_{1-\alpha}} + o(1) \quad (64)$$

On the one hand, for any finite $k \in \mathbb{N}$, we have

$$n \int_{1-\tau_n^*}^1 \frac{G_n(x)}{G_n(1-\tau_n^*)} dx \quad (65)$$

$$\geq n \int_{1-\tau_n^*}^{1-\tau_n^* + \frac{k}{n}} \frac{G_n(x)}{G_n(1-\tau_n^*)} dx$$

$$= n \int_0^{\frac{k}{n}} \exp(-ns_{1-\tau_n^*}x) dx \cdot (1+o(1)) \quad (66)$$

$$= \frac{1 - \exp(-ks_{1-\tau_n^*})}{s_{1-\alpha}} (1+o(1)). \quad (67)$$

(46), (64) and (67) complete the proof of Theorem 2.

APPENDIX C PROOF OF THEOREM 3

It should be noted that:

$$\begin{aligned} & \log(\overline{\text{SG}}_{\text{VLC}}(n; \alpha)) + \log(2\alpha) \\ &= \frac{1}{n} \log(\text{vol}(\mathcal{T}_n(t_n^*))) \\ &= \frac{1}{n} \log(G_n(1-\tau_n^*)) \\ &= \frac{1}{n} \log\left(\frac{\exp(nL(1-\tau_n^*))}{\sqrt{2\pi n}D(1-\tau_n^*)} (1+o(1))\right) \end{aligned} \quad (68)$$

$$\begin{aligned} &= L\left(1 - \alpha - \frac{1}{\mu^*} \frac{1}{n} + o\left(\frac{1}{n}\right)\right) + o\left(\frac{1}{n}\right) \\ &\quad - \frac{1}{n} \log\left(\sqrt{2\pi n}D\left(1 - \alpha - \frac{1}{\mu^*} \frac{1}{n} + o\left(\frac{1}{n}\right)\right)\right) \end{aligned} \quad (69)$$

$$\begin{aligned} &= L(1-\alpha) - \frac{\log(2\pi n)}{2n} + \frac{1}{n}(1 - \log(D(1-\alpha))) + o\left(\frac{1}{n}\right) \end{aligned} \quad (70)$$

$$\begin{aligned} &= h_{\max}(\alpha) - \frac{\log(n)}{2n} + o\left(\frac{1}{n}\right) \\ &\quad + \frac{1}{n} \left(1 - \frac{1}{2} \log\left(2\pi\left(-\mu^* + 2\alpha\mu^* + (\mu^*)^2\alpha(1-\alpha)\right)\right)\right) \end{aligned} \quad (71)$$

$$= h_{\max}(\alpha) - \log(2\alpha) - \frac{\log(n)}{2n} + \frac{\omega_\alpha}{n} + o\left(\frac{1}{n}\right) \quad (72)$$

where Eq. (68) is obtained by Eq. (51), Eq. (69) is derived from Theorem 2 Eq. (70) is calculated by

$$\begin{aligned} & L\left(1 - \alpha - \frac{1}{\mu^*} \frac{1}{n} + o\left(\frac{1}{n}\right)\right) \\ &= L(1-\alpha) + L'(1-\alpha) \left(-\frac{1}{\mu^*} \frac{1}{n} + o\left(\frac{1}{n}\right)\right) + o\left(\frac{1}{n}\right) \\ &= L(1-\alpha) - s_{1-\alpha} \left(-\frac{1}{\mu^*} \frac{1}{n}\right) + o\left(\frac{1}{n}\right) \\ &= L(1-\alpha) + \frac{1}{n} + o\left(\frac{1}{n}\right), \end{aligned} \quad (73)$$

and $D\left(1 - \alpha - \frac{1}{\mu^*} \frac{1}{n} + o\left(\frac{1}{n}\right)\right) = D(1-\alpha) + o(1)$, and Eq. (71) can be obtained by substitute the value into $L(1-\alpha)$ and $D(1-\alpha)$.

REFERENCES

- [1] Y.-Y. Zhang, "Intrinsic robustness of MISO visible light communications: Partial CSIT can be as useful as perfect one," *IEEE Transactions on Communications*, vol. 67, no. 2, pp. 1297–1312, 2019.
- [2] X. Zhu, C.-X. Wang, J. Huang, M. Chen, and H. Haas, "A novel 3D non-stationary channel model for 6G indoor visible light communication systems," *IEEE Transactions on Wireless Communications*, vol. 21, no. 10, pp. 8292–8307, 2022.
- [3] A. Kafizov, A. Elzanaty, and M.-S. Alouini, "Probabilistic shaping-based spatial modulation for spectral-efficient VLC," *IEEE Transactions on Wireless Communications*, vol. 21, no. 10, pp. 8259–8275, 2022.
- [4] A. Mostafa and L. Lampe, "Optimal and robust beamforming for secure transmission in MISO visible-light communication links," *IEEE Transactions on Signal Processing*, vol. 64, no. 24, pp. 6501–6516, 2016.
- [5] J.-B. Wang, Q.-S. Hu, J. Wang, M. Chen, and J.-Y. Wang, "Tight bounds on channel capacity for dimmable visible light communications," *Journal of Lightwave Technology*, vol. 31, no. 23, pp. 3771–3779, 2013.
- [6] P. A. Loureiro, G. M. Fernandes, S. F. H. Correia, R. A. S. Ferreira, F. P. Guiomar, and P. P. Monteiro, "Multi-gigabit RGB-VLC transmission with jointly optimized lighting and communications," *Journal of Lightwave Technology*, pp. 1–8, 2024.
- [7] J. M. Kahn and J. R. Barry, "Wireless infrared communications," vol. 85, pp. 265–298, Feb. 1997.
- [8] S. Hranilovic, *Wireless Optical Communication Systems*. 2005.
- [9] A. Chaaban, Z. Rezki, and M.-S. Alouini, "Capacity bounds and high-SNR capacity of MIMO intensity-modulation optical channels," *IEEE Transactions on Wireless Communications*, vol. 17, no. 5, pp. 3003–3017, 2018.
- [10] L. Li, S. M. Moser, L. Wang, and M. Wigger, "On the capacity of MIMO optical wireless channels," *IEEE Transactions on Information Theory*, vol. 66, no. 9, pp. 5660–5682, 2020.
- [11] R.-H. Chen, L. Li, J. Zhang, W. Zhang, and J. Zhou, "On the capacity of MISO optical intensity channels with per-antenna intensity constraints," *IEEE Transactions on Information Theory*, vol. 68, no. 6, pp. 3920–3941, 2022.

- [12] A. Chaaban, Z. Rezki, and M.-S. Alouini, "On the capacity of intensity-modulation direct-detection Gaussian optical wireless communication channels: A tutorial," *IEEE Communications Surveys & Tutorials*, vol. 24, no. 1, pp. 455–491, 2022.
- [13] J. Karout, G. Kramer, F. R. Kschischang, and E. Agrell, "A two-dimensional signal space for intensity-modulated channels," *IEEE Communications Letters*, vol. 16, no. 9, pp. 1361–1364, 2012.
- [14] D. Zhang and S. Hranilovic, "Bandlimited optical intensity modulation under average and peak power constraints," *IEEE Transactions on Communications*, vol. 64, no. 9, pp. 3820–3830, 2016.
- [15] Y.-Y. Zhang, H.-Y. Yu, and J.-K. Zhang, "Block precoding for peak-limited MISO broadcast VLC: Constellation-optimal structure and addition-unique designs," *IEEE Journal on Selected Areas in Communications*, vol. 36, no. 1, pp. 78–90, 2018.
- [16] R. Zamir, *Lattice Coding for Signals and Networks*. Cambridge University Press, 2014.
- [17] D.-S. Shiu and J. Kahn, "Shaping and nonequiprobable signaling for intensity-modulated signals," *IEEE Transactions on Information Theory*, vol. 45, no. 7, pp. 2661–2668, 1999.
- [18] Y.-Y. Zhang, H.-Y. Yu, J.-K. Zhang, Y.-J. Zhu, and T. Wang, "Energy-efficient space-time modulation for indoor MISO visible light communications," *Optics Letters*, vol. 41, pp. 329–332, Jan 2016.
- [19] A. A. Farid and S. Hranilovic, "Channel capacity and non-uniform signalling for free-space optical intensity channels," *IEEE Journal on Selected Areas in Communications*, vol. 27, pp. 1553–1563, Dec. 2009.
- [20] A. Al-Kinani, J. Sun, C.-X. Wang, W. Zhang, X. Ge, and H. Haas, "A 2-D non-stationary GBSM for vehicular visible light communication channels," *IEEE Transactions on Wireless Communications*, vol. 17, no. 12, pp. 7981–7992, 2018.
- [21] H. Yang, W.-D. Zhong, C. Chen, A. Alphones, P. Du, S. Zhang, and X. Xie, "Coordinated resource allocation-based integrated visible light communication and positioning systems for indoor IoT," *IEEE Transactions on Wireless Communications*, vol. 19, no. 7, pp. 4671–4684, 2020.
- [22] H. Zhou, M. Zhang, and X. Ren, "Design and implementation of wireless optical access system for VLC-IoT networks," *Journal of Lightwave Technology*, vol. 41, no. 8, pp. 2369–2380, 2023.
- [23] E. Niarchou, A. C. Boucouvalas, Z. Ghassemlooy, L. N. Alves, and S. Zvanovec, "Visible light communications for 6G wireless networks," in *2021 Third South American Colloquium on Visible Light Communications (SACVLC)*, pp. 01–06, 2021.
- [24] S. Chang, N. Huang, C. Gong, and X.-Y. Li, "Low-latency network slicing for VLC-based industrial internet of things: Superframe duration minimization and delay violation probability analysis," *IEEE Internet of Things Journal*, vol. 10, no. 18, pp. 16617–16636, 2023.
- [25] S. Hranilovic, "Minimum-bandwidth optical intensity nyquist pulses," *IEEE Transactions on Communications*, vol. 55, no. 3, pp. 574–583, 2007.
- [26] G. R. Lang and F. M. Longstaff, "A Leech lattice modem," *IEEE Journal on Selected Areas in Communications*, vol. 7, pp. 968–973, Aug. 2002.
- [27] Z. Qu and I. B. Djordjevic, "On the probabilistic shaping and geometric shaping in optical communication systems," *IEEE Access*, vol. 7, pp. 21454–21464, 2019.
- [28] A. Amari, S. Goossens, Y. C. Gültekin, O. Vassilieva, I. Kim, T. Ikeuchi, C. M. Okonkwo, F. M. J. Willems, and A. Alvarado, "Introducing enumerative sphere shaping for optical communication systems with short blocklengths," *Journal of Lightwave Technology*, vol. 37, pp. 5926–5936, Dec 2019.
- [29] R.-H. Chen, J. Zhang, and Y.-Y. Zhang, "FFT-assisted coded modem for intensity-modulated signals under peak and average power constraints," *IEEE Transactions on Communications*, vol. 68, no. 1, pp. 274–288, 2020.
- [30] M. Hayashi, "Information spectrum approach to second-order coding rate in channel coding," *IEEE Transactions on Information Theory*, vol. 55, no. 11, pp. 4947–4966, 2009.
- [31] Y. Polyanskiy, H. V. Poor, and S. Verdú, "Channel coding rate in the finite blocklength regime," *IEEE Transactions on Information Theory*, vol. 56, pp. 2307–2359, May 2010.
- [32] T. Komine and M. Nakagawa, "Fundamental analysis for visible-light communication system using LED lights," *IEEE Transactions on Consumer Electronics*, vol. 50, no. 1, pp. 100–107, 2004.
- [33] G. Forney, "A bounded-distance decoding algorithm for the Leech lattice, with generalizations," *IEEE Transactions on Information Theory*, vol. 35, no. 4, pp. 906–909, 1989.
- [34] F. Kschischang and S. Pasupathy, "Optimal shaping properties of the truncated polydisc," *IEEE Transactions on Information Theory*, vol. 40, no. 3, pp. 892–903, 1994.
- [35] G. D. Forney, Jr. and L.-F. Wei, "Multidimensional constellations—Part I: Introduction, figures of merit, and generalized cross constellations," *IEEE Journal on Selected Areas in Communications*, vol. 7, pp. 877–892, Aug. 1989.
- [36] A. Lapidath, S. M. Moser, and M. A. Wigger, "On the capacity of free-space optical intensity channels," *IEEE Transactions on Information Theory*, vol. 55, no. 10, pp. 4449–4461, 2009.
- [37] A. Ingber, R. Zamir, and M. Feder, "Finite-dimensional infinite constellations," *IEEE Transactions on Information Theory*, vol. 59, no. 3, pp. 1630–1656, 2013.
- [38] S. Shamai (Shitz) and I. Bar-David, "The capacity of average and peak-power-limited quadrature Gaussian channels," *IEEE Transactions on Information Theory*, vol. 41, no. 4, pp. 1060–1071, 1995.
- [39] H.-A. Loeliger, "Averaging bounds for lattices and linear codes," *IEEE Transactions on Information Theory*, vol. 43, no. 6, pp. 1767–1773, 1997.
- [40] J. Conway and N. J. A. Sloane, *Sphere Packings, Lattices and Groups*. 3rd ed., 1999.
- [41] H. Cohn, A. Kumar, S. D. Miller, D. Radchenko, and M. Viazovska, "The sphere packing problem in dimension 24," *Annals of Mathematics*, vol. 185, no. 3, pp. 1017–1033, 2017.
- [42] G. Forney, "Coset codes. I. introduction and geometrical classification," *IEEE Transactions on Information Theory*, vol. 34, no. 5, pp. 1123–1151, 1988.
- [43] O. Amrani, Y. Be'ery, A. Vardy, F.-W. Sun, and H. van Tilborg, "The Leech lattice and the Golay code: bounded-distance decoding and multilevel constructions," *IEEE Transactions on Information Theory*, vol. 40, no. 4, pp. 1030–1043, 1994.
- [44] L. Li, R.-H. Chen, Y.-Y. Zhang, J.-N. Guo, and J. Zhang, "Space-time constellation for MU-MISO dimmable visible light communications," *IEEE Communications Letters*, vol. 25, no. 7, pp. 2329–2332, 2021.
- [45] H. Ma, L. Lampe, and S. Hranilovic, "Coordinated broadcasting for multi-user indoor visible light communication systems," *IEEE Transactions on Communications*, vol. 63, no. 9, pp. 3313–3324, 2015.
- [46] V. V. Petrov, "On the probabilities of large deviations for sums of independent random variables," *Theory of Probability & Its Applications*, vol. 10, no. 2, pp. 287–298, 1965.